Lamb Wave-Mode Tuning of Piezoelectric Wafer Active Sensors for Structural Health Monitoring

Giola B. Santoni
Graduate Research Assistant
e-mail: bottai@engr.sc.edu

Lingyu Yu
Graduate Research Assistant
e-mail: Yu3@engr.sc.edu

Buli Xu
Graduate Research Assistant
e-mail: Xub@engr.sc.edu

Victor Giurgiutiu
Professor
e-mail: victorg@sc.edu

Department of Mechanical Engineering,
University of South Carolina,
Columbia, SC 29208

An analytical and experimental investigation of the Lamb wave-mode tuning with piezoelectric wafer active sensors (PWASs) is presented. The analytical investigation assumes a PWAS transducer bonded to the upper surface of an isotropic flat plate. Shear lag transfer of tractions and strains is assumed, and an analytical solution using the spacewise Fourier transform is reviewed, closed-form solutions are presented for the case of ideal bonding (i.e., load transfer mechanism localized at the PWAS boundary). The analytical solutions are used to derive Lamb wave-mode tuning curves, which indicate that frequencies exist at which the A0 mode or the S0 mode can be either suppressed or enhanced. Extensive experimental tests that verify these tuning curves are reported. The concept of "effective PWAS dimension" is introduced to account for the discrepancies between the ideal bonding hypothesis and the actual shear-lag load transfer mechanism. The paper further shows that the capability to excite only one desired Lamb wave mode is critical for practical structural health monitoring (SHM) applications such as PWAS phased array technique (e.g., the embedded ultrasonics structural radar (EUSR)) and the time reversal process (TRP). In PWAS phased array EUSR applications, the basic assumption of the presence of a single low-dispersion Lamb wave mode (S0) is invoked since several Lamb wave modes traveling at different speeds would disturb the damage imaging results. Examples are given of correctly tuned EUSR images versus detuned cases, which illustrate the paramount importance of Lamb wave-mode tuning for the success of the EUSR method. In the TRP study, an input wave packet is reconstructed at a transmission PWAS when the signal recorded at the receiving PWAS is reversed in the time domain and transmitted back to the original PWAS. Ideally, TRP could be used for damage detection without a prior baseline. However, the application of TRP to Lamb waves SHM is impended by the dispersive and multimodal nature of the Lamb waves. The presence of more then one mode usually produces additional wave packets on both sides of the original wave packet due to the coupling of the Lamb wave modes. The PWAS Lamb wave tuning technique described in this paper is used to resolve the side packets problem. Several tuning cases are illustrated. It is found that the 30 kHz tuning of the A0 Lamb wave mode with a 16-count smoothed tone burst leads to the complete elimination of the side wave packets. However, the elimination was less perfect for the 290 kHz tuning of the S0 mode due to the frequency sidebands present in the tone-burst wave packet. [DOI: 10.1115/1.2748469]

Keywords: structural health monitoring, SHM, Lamb waves, piezoelectric wafer active sensor, PWAS, tuning, sensors phased array, time reversal process, embedded ultrasonics structural radar, EUSR

1 Introduction

An analytical and experimental investigation of Lamb wave-mode tuning with piezoelectric wafer active sensors (PWAS) is presented. The analytical investigation assumes PWAS bonded to the upper surface of an isotropic flat plate. Shear lag transfer of tractions and strains is assumed, an analytical solution using the spacewise Fourier transform is reviewed, and closed-form solutions are presented for the case of ideal bonding. The analytical solutions are used to derive Lamb wave-mode tuning curves, which indicate that frequencies exist at which the A0 mode or the S0 mode can be either suppressed or enhanced. Extensive experimental tests that verify these tuning curves are reported. The con-

cept of "effective PWAS dimension" is introduced to account for the discrepancies between the ideal bonding hypothesis and the actual shear-lag load transfer mechanism. The paper further shows that the capability to excite only one desired Lamb wave mode is critical for practical applications, such as PWAS phased array technique and the time reversal process. In PWAS phased array applications, the assumption of the presence of a single low-dispersion Lamb wave mode (S0) is invoked since several Lamb wave modes traveling at different speeds would disturb the damage imaging results. Examples are given of correctly tuned EUSR images versus detuned cases, which illustrate the paramount importance of Lamb wave-mode tuning. In the TRP study, an input wave packet is reconstructed at a transmission PWAS when the signal recorded at the receiving PWAS is reversed in the time domain and transmitted back to the original PWAS. Ideally, TRP could be used for damage detection without a prior baseline. However, the application of TRP to Lamb waves structural health

Copyright © 2007 by ASME   **Transactions of the ASME**
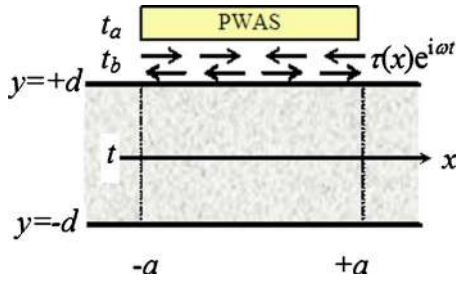
Fig. 1 Layer interaction between the PWAS and the structure modeling [3]

Fig. 2 Variation of shear-lag transfer mechanism with bond thickness t_b for a APC-850 PWAS (E_a=63 GPa, t_a=0.2 mm, l_a =7 mm, d_{31}=−175 mm/kV) attached to a thin-wall aluminum structure (E=70 GPa and t=1 mm) through a bond layer of G_b =2 GPa (normalized position covers a half-PWAS length from center outward)

monitoring (SHM) is impended by the dispersive and multimodal nature of the Lamb waves. The presence of more then one mode usually produces additional wave packets on both sides of the original wave packet due to the coupling of the Lamb wave modes. The PWAS Lamb wave tuning technique described in this paper is used to resolve the side packets problem. Several tuning cases are illustrated. It is found that the 30 kHz tuning of the A0 Lamb wave mode with a 16-count smoothed tone burst leads to the complete elimination of the side wave packets. However, the elimination was less perfect for the 290 kHz tuning of the S0 mode due to the frequency sidebands present in the tone-burst wave packet.

2   PWAS Lamb Wave Tuning on plates

The tuning of a particular mode is quite important in structural health monitoring. Of particular interest is the interaction of PWAS and structure together. The coupling between PWAS and structures has been studied Crawley and de Luis [1], by Crawley and Anderson [2], and Giurgiutiu [3]. Figure 1 shows the PWAS bonded to the plate. Assume the PWAS has elastic modulus E_a and thickness t_a, while the structure has elastic modulus E and thickness t, and the bond layer has shear modulus G_b and thickness t_b. The bond layer acts as a shear layer in which the mechanical effects are transmitted through the shear effects.

With this model, the interfacial shear stress in bonding layer is expressed through

$$\tau(x) = \frac{t_a}{a}\frac{\psi}{\alpha+\psi}E_a\varepsilon_{\text{ISA}}\left(\Gamma a\frac{\sinh\Gamma x}{\cosh\Gamma a}\right) \tag{1}$$

where α is a coefficient that depends on the frequency, phase velocity, and plate thickness, and, hence, on the strain distribution across the plate thickness. For low-frequency dynamic conditions, α can be taken equal to 4 (symmetric and antisymmetric 0 modes can be approximated, respectively, with axial and flexural waves). Coefficient $\psi = Et/E_a t_a$ represents the maximum fraction of the piezoelectric strain that can be induced in the structure; ε_{ISA} is the induced strain in the PWAS by an electric voltage; Γ^2 is the shear lag parameter and it indicates the effectiveness of the shear transfer. Γ is influenced by the stiffness and thickness of the bonding layer t_b. A characteristic plot of the interfacial shear stress along the length of the PWAS for different thickness of the bonded layers is represented in Fig. 2. For a thin layer of the bonded material (1 μm), the shear stress is transmitted to the structure only at the ends of the PWAS. This is the ideal bonding solution, which can be considered true as a first approach to the problem. In this case, the shear stress in the bonding layer can be expressed as

$$\tau(x) = a\tau_0[\delta(x-a)-\delta(x+a)] \tag{2}$$

When the PWAS is coupled with the structure, the actuator and the structure may extend, bend, and shear. The relatively importance of one of the three modes depends on the geometry and the stiffness of the structure, the PWAS, and the bonding layer. We assume that the bonding between the PWAS and the structure is
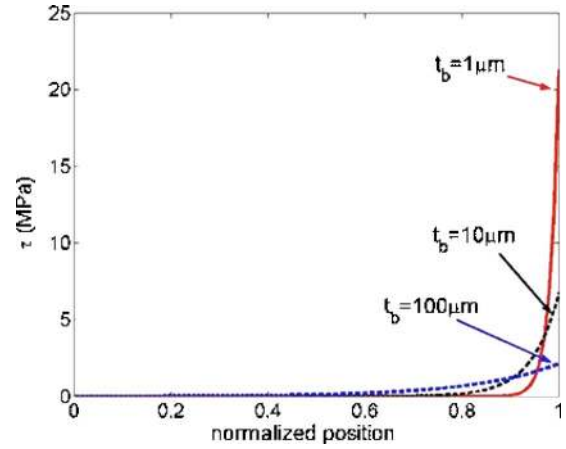
ideal; hence, only the interaction between the PWAS and the plate is of interest and the load is transferred at the ends of the PWAS.

To investigate the tuning of the two elements two different kinds of methods can be used: the classical integral transform method as developed by Giurgiutiu [3] for 1D PWAS and by Raghavan and Cesnik [4,5] for circular PWAS and 3D PWAS; and the modal normal expansion technique (MNE), as developed by Auld [6], where the fields generated in the structure due to the application of the surface loading are expanded in the form of an infinite series of the normal modes of the structure itself. In both techniques, the velocity field of the modes must be known, and it is important to clearly define the physical properties of the sources used to generate the waves. In Sec. 2.1, an overview of the integral transform technique and some interesting experimental results that validate the theoretical results will be presented.

2.1   PWAS-Lamb Wave Interaction via the Integral Transform Technique. The integral transform technique for the case of infinite PWAS strip bonded with a finite adhesive layer to a plate was first developed by Giurgiutiu [3]. He assumed the harmonic load distribution (2) for the case of an ideal bonding solution. This assumption led to a harmonic solution of the wave equation itself. The wave equation in terms of potential function was solved by transforming it with the Fourier transform, and the displacement solution was found. The problem was divided into symmetric and antisymmetric solutions (the plate under investigation was isotropic). The boundary conditions applied were as represented in Fig. 3. Once the integration constants were derived, the strain equations were transformed to the space domain with an inverse Fourier transformation. The inversion required the use of the theorem of the residues,

$$\varepsilon_x(x,t)|_{y=d} = -i\frac{a\tau_0}{\mu}\left[\sum_{\xi^S}\sin(\xi^S a)\frac{N_S(\xi^S)}{D'_S(\xi^S)}e^{-i(\xi^S x-\omega t)}\right.$$
$$\left.+\sum_{\xi^A}\sin(\xi^A a)\frac{N_A(\xi^A)}{D'_A(\xi^A)}e^{-i(\xi^A x-\omega t)}\right] \tag{3}$$

where

$$N_S = \xi\beta(\xi^2+\beta^2)\cos(\alpha d)\cos(\beta d);\quad N_A = \xi\beta(\xi^2$$
$$+\beta^2)\sin(\alpha d)\sin(\beta d) \tag{4}$$

$$D_S = (\xi^2-\beta^2)^2\cos(\alpha d)\sin(\beta d)+4\xi^2\alpha\beta\sin(\alpha d)\cos(\beta d) \tag{5}$$
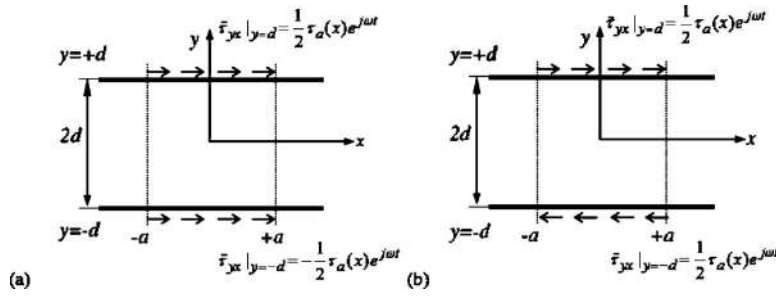
Fig. 3 Load on a plate due to the PWAS actuation: (*a*) symmetric and (*b*) asntisymmetric [3]

$$D_A = (\xi^2 - \beta^2)^2 \sin(\alpha d)\cos(\beta d) + 4\xi^2 \alpha\beta \cos(\alpha d)\sin(\beta d) \quad (6)$$

ξ^S and ξ^A are the zeros of the Rayleigh-Lamb equations for symmetric and antisymmetric mode, respectively,

$$\frac{\tan(\beta d)}{\tan(\alpha d)} = -\left[\frac{4\xi^2 \alpha\beta}{(\xi^2 - \beta^2)^2}\right]^{\pm 1} \quad (7)$$

where d is the half thickness of the plate, $\alpha^2 = (\omega^2/c_p^2) - \xi^2$; $\beta^2 = (\omega^2/c_S^2) - \xi^2$ and $\xi^2 = \omega^2/c^2$, c_p is the pressure velocity, c_s is the shear velocity, c is the unknown phase velocity, and ξ is the wavenumber in the x and r directions, respectively. The plus in Eq. (7) is for the symmetric case and the minus for the antisymmetric case.

From the derived strain equation, the displacement equation was calculated,

$$u_x(x,t)|_{y=d} = -\frac{a^2 \tau_0}{\mu}\left[\sum_{\xi^S} \frac{\sin(\xi^S a)}{\xi^S a}\frac{N_S(\xi^S)}{D_S'(\xi^S)}e^{-i(\xi^S x - \omega t)}\right.$$
$$\left. + \sum_{\xi^A} \frac{\sin(\xi^A a)}{\xi^A a}\frac{N_A(\xi^A)}{D_A'(\xi^A)}e^{-i(\xi^A x - \omega t)}\right] \quad (8)$$

Raghavan and Cesnik [4] had extended these 1D results to the case of a circular crested Lamb waves. The resulting expression of the displacement has Bessel and Henkel function instead of sine and exponential functions, i.e.,

$$u_r(r,t)|_{z=d} = -\pi i \frac{a\tau_0}{\mu}e^{i\omega t}\left[\sum_{\xi^S} J_1(\xi^S a)\frac{N_S(\xi^S)}{D_S'(\xi^S)}H_1^{(2)}(\xi^S r)\right.$$
$$\left. + \sum_{\xi^A} J_1(\xi^A a)\frac{N_A(\xi^A)}{D_A'(\xi^A)}H_1^{(2)}(\xi^A r)\right] \quad (9)$$

The strain can be derived from Eq. (9) as

$$\varepsilon_r(r,t)|_{z=d} = \frac{\partial u_r(r,t)|_{z=d}}{\partial r} \quad (10)$$

Figure 4 represent a simulation of Eq. (3). It is noted that the normalize strain curves follow the general pattern of a sine function, which hits zeros when the half length of the PWAS match an odd multiple of one of the wavenumbers of the Lamb waves plate. As indicated in Fig. 4, such zeros occurred at different frequencies for the A0 mode than for the S0 mode. Raghavan and Cesnik [5] have also developed the integral form solution for 3D PWAS. In this case, the equation of motion is a function of three space variables. In order to ease the solution of the problem, they used the double Fourier transform. The theoretical procedure is similar to that of 2D model; however, the transformation back to the space domain is quite difficult. For this motive, the authors only considered some particular configurations, such as rectangular and ring-shaped piezoelectric actuators.

2.2 Experimental Validation of PWAS Lamb Wave Tuning. Experiments have been performed on different plate thicknesses and PWAS shapes (Fig. 5) to validate the theoretical formulae presented in the previous section. The signal used was a Hanning windowed tone burst with three counts. The signal was generated by a function generator (Hewlett Packard 33120A) and sent through an amplifier (Krohn-Hite) to a transmitter PWAS. A digital oscilloscope (Tektronix TDS5034B) was used to measure the signal captured at the receiver PWAS. Several plates were used for these experiments: (i) aluminum alloy 2024-T3 1.07 mm thickness 1222×1063 mm; (ii) aluminum alloy 6061-T8
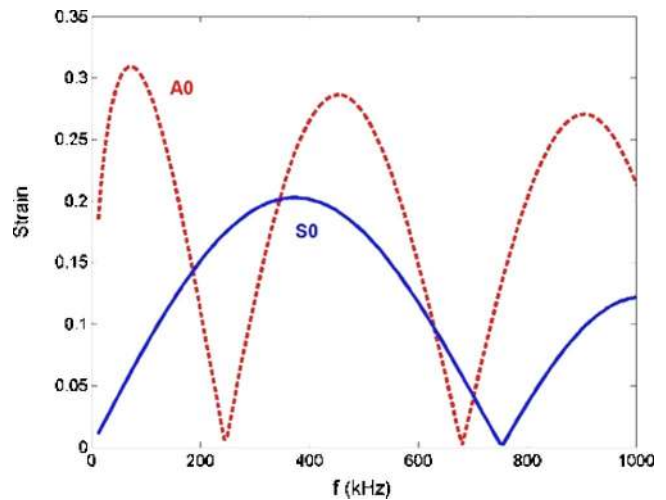

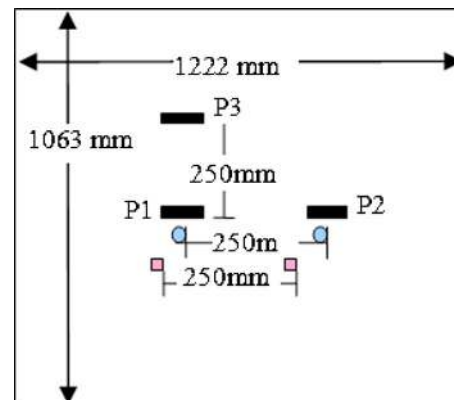**Fig. 4 Predicted Lamb wave response of a 1.6 mm aluminum plate under a 7 mm PWAS excitation: strain response**

Fig. 5 Aluminum plate 2024-T3 1.07 mm with square, rectangular, and round PWASs
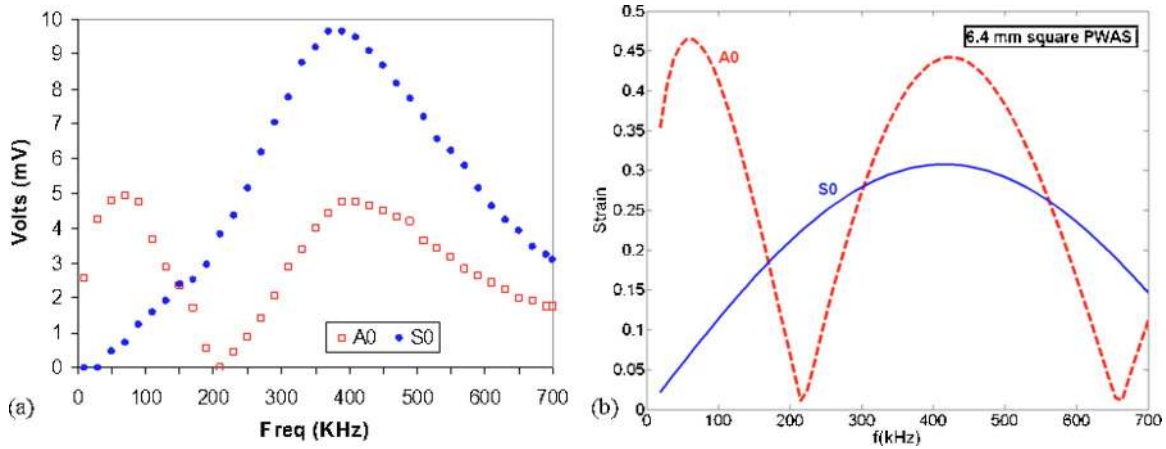
Fig. 6 Tuning: Aluminum 2024-T3, 1.07 mm thickness, 7 mm square PWAS: (*a*) experimental data and (*b*) prediction with Eq. (3)

3.175 mm thickness 505 × 503 mm, and (iii) aluminum alloy 2024-T3 3.15 mm thickness 1209 × 1209 mm. In each experiment, we used two PWASs at a distance 250 mm from each other. One PWAS was used as transmitter and the other as receiver. The frequency of the signal was swept from 10 kHz to 700 kHz in steps of 20 kHz. In this frequency range, for the 1.07 mm thickness plate, only S0 and A0 modes were present; whereas for the 3.175 mm and 3.15 mm thick plates, the S0, A0, and A1 modes were present. For each frequency, the wave amplitude and the time of flight for both the symmetric S0 mode and the antisymmetric A0 and A1 modes were collected. From these readings, we computed the group velocity for each mode.

2.2.1 Square PWAS Tuning. In these experiments we used a square PWAS of 7 mm long, 0.2 mm thick (American Piezo Ceramics APC-850).

2.2.1.1 Experiments on aluminum alloy 2024-T3 1.07 mm thickness 1222 × 1063 mm. Figure 5 shows the conuration for the square PWAS on the plate aluminum alloy 2024-T3 1.07 mm thickness. The PWAS were located at the center of the plate in order to avoid interference with the reflection from the boundaries.

Figure 6(*a*) shows the experimental data of the wave amplitude for the S0 and A0 modes. Figure 6(*b*) shows the predicted values of the wave amplitude for S0 and A0 modes for a PWAS with effective length of 6.4 mm. For this effective PWAS length value, we obtained the best agreement between experiments and predictions. In the development of the theory, it was assumed that there was ideal bonding between the PWAS and the plate. This assumption means that the stresses between the transducers and the plate are fully transferred at the PWAS ends. In reality, the stresses are transferred over a region adjacent to the PWAS ends (Fig. 2). The experimental and theoretical values of the tuning were brought in good agreement by using the equivalent PWAS length value (Figs. 6(*a*) and 6(*b*)). The first maximum of the A0 mode happened at around 60 Hz, at which frequency the S0 mode is very small. This behavior was correspondingly observed experimentally. The first minimum of the A0 mode, both in the experimental graph and in the predicted graph, was found around 210 kHz. At this frequency, the S0 mode amplitude is nonzero and placed on an increasing curve. Thus, at this frequency, the S0 signal was dominant. In addition, the theory also predicts that the S0 maximum would happen at 425 kHz, which is the same frequency as that of the second A0 maximum; this prediction was also verified by the experiments.

2.2.1.2 Experiments on aluminum alloy 2024-T3 3.15 mm thickness 1209 × 1209 mm. Experiments have been performed on plates of thickness 3.15 mm. In these cases, at frequencies between 500 kHz and 700 kHz, the modes present were S0, A0, and A1. Their velocities were close to one another, and the S0 and A1 modes were both dispersive at the frequency-thickness product values. Figures 7(*a*) and 7(*b*) show, respectively, the experimental data and the predicted values of the amplitude of the A0, S0, and A1 wave for an aluminum plate 2024-T3 3.15 mm thickness 1209 × 1209 mm. The experimental and predicted values are in accordance up to 550 kHz. The S0 maximum is close to the A0 minimum in both representations. The A1 mode can be detected.

2.2.2 Rectangular PWAS Tuning. Rectangular PWAS of high aspect ratio were tested to examine the directional tuning of Lamb waves. Three rectangular PWAS of 25 mm × 5 mm long and 0.15 mm thickness (Steiner & Martin) were used. The experiment configuration is shown in Fig. 5. PWAS P1 was the transmitter and PWAS P2 and P3 were the receivers. Only the experiment from PWAS P1 to PWAS P2 is reported for brevity. Figure 8(*a*) shows the experimental values of the wave amplitude for frequencies up to 250 kHz taken with steps of 3 kHz. The small steps used to collect the data allowed detection of the three maxima in the A0 mode. The first two maxima are in accordance with the predicted values, while the third is at a higher frequency than that predicted. The S0 maximum is in accordance with the predicted values (Fig. 8(*b*)). The value of the theoretical PWAS that best predicts the experimental behavior is 24.8 mm. It is interesting to note that when the receiver is along the line of the larger dimension of the transmitter, the PWAS behaves as a square PWAS (i.e., 25 mm × 25 mm).

2.2.3 Effective PWAS Length Values. During the experiments, it was noted that the best concordance between the experimental data and the predicted curves was achieved for a theoretical PWAS length smaller than that of the real transducer. In particular, it was found that as the length of the PWAS decreases, the percentage of noneffective area of the transducer increases. Table 1 shows the values of the real PWAS length, the effective values used in the theoretical predictions and the percentages of the effective length of the real PWAS and the complimentary noneffective length.

While the rectangular PWAS along its greatest dimension (25 mm) transmits stress to the plate very close to its borders, the same PWAS in the smallest dimension (5 mm) transmits the stress to the plate at 5% of its length before the borders. The adjustment
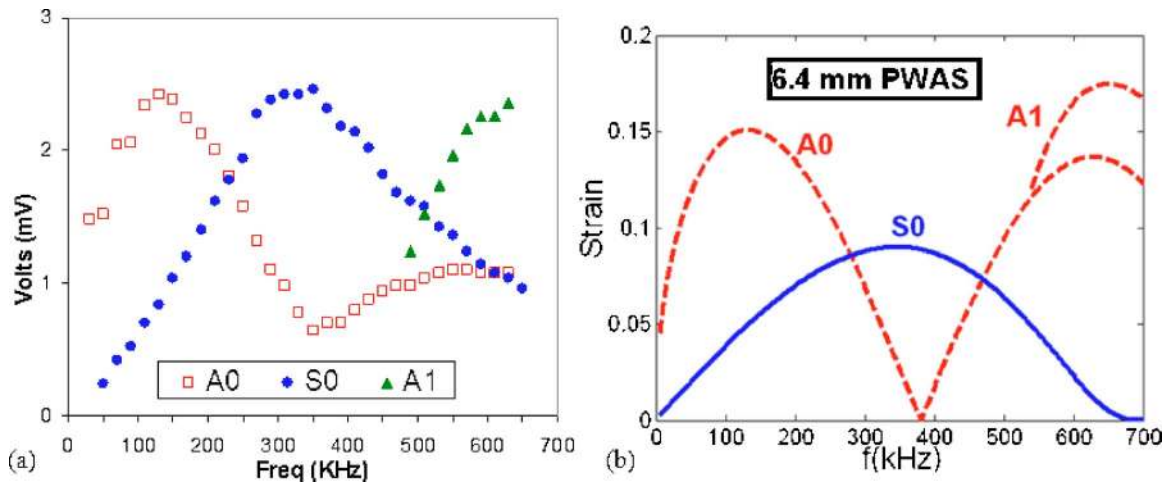
Fig. 7 Aluminum 2024-T3, 3.15 mm thickness, 7 mm square PWAS: (*a*) experimental data and (*b*) prediction (Eq. (3))

of the PWAS length was necessary because the theoretical formulas supposed that the stress induced by the PWAS was transferred to the structure only at the end of the PWAS. The experiments have shown that this assumption is not entirely true and that the theory must include the actual shear stress transmission mechanism. However, in lieu of a more complete theory, we have developed here the concept of effective PWAS length, as indicated in Table 1.

3 Applications

The use of tuned Lamb wave modes in structural health monitoring is very important because it permits the researchers to address the detection of specific defects with specific Lamb wave modes. First, we explored the use of a PWAS phased array and tuned S0 mode Lamb waves to create sweeping beams that can interrogate a large area from a single location. Next, we verified

that the ability of tuning certain Lamb wave modes is very important for using time reversal method to perfectly reconstruct the input excitation.

3.1 Phase Array. The phased array application of the PWAS transducers allows large structural areas to be monitored from a single location. The phased array application utilizes the beam steering concepts based on differentially firing various elements of the phased array such that constructive/destructive interference of all the transducers forms a wave beam in a certain direction. The phased array concept was initially developed for radar applications where it operates with single-mode electromagnetic waves. The phased array concept was transitioned to PWAS-coupled Lamb waves by Giurgiutiu and Bao [7] under the name "embedded ultrasonics structural radar" (EUSR). The EUSR principles and initial results were reported extensively in Ref. [7]. Using
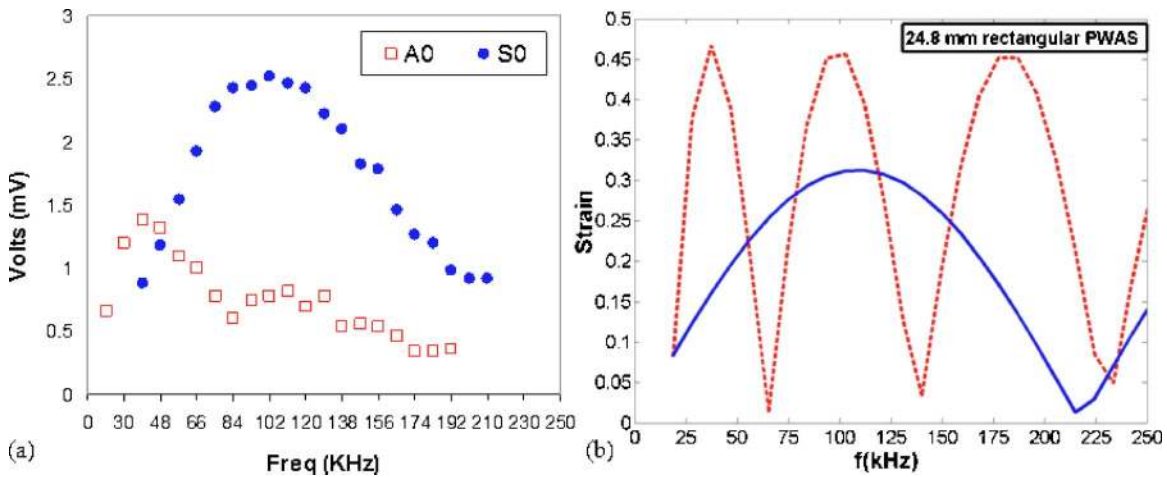

Fig. 8 Tuning on plate 2024-T3, 1.07 mm thick, rectangular PWAS (P1-P2): (*a*) experimental data and (*b*) prediction with Eq. (3)

Table 1 PWAS effective length

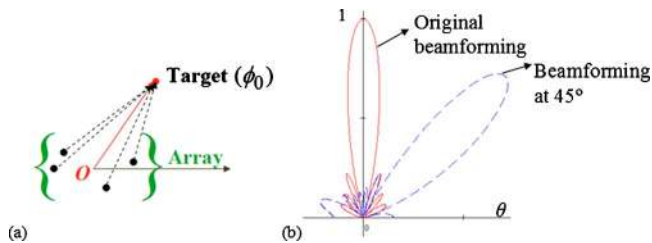| Real PWAS length (mm)	Effective PWAS length (mm)	Percent of effective PWAS (%)	Percent of noneffective PWAS (%)
25	24.8	99.2	0.8
7	6.4	91.4	8.6
5	4.5	90	10

Fig. 9 PWAS phased array interrogation: (*a*) illustration of a PWAS phased array to be directed to a certain direction and (*b*) beamforming of a PWAS array using eight PWAS aligned along a straight line

Lamb waves propagating as guided waves in thin-wall plate and shell structures allows monitoring of large structural areas from a single location in which the PWAS phased array is placed. This concept can be applied to various thin-wall structures, such as aircraft, storage tanks, large pipes, etc. The main challenge in this application (as different from the electromagnetic radar) is the fact that Lamb waves are basically multimode and generally dispersive. However, these multimodal and dispersive challenges can be successfully alleviated through the use of Lamb wave tuning, as described next.

3.1.1 PWAS Guided Lamb Wave Phased Array. The concept of PWAS guided Lamb wave phased array utilizes an array of M closely spaced PWAS that are permanently attached to the structures (Fig. 9(*a*)) and interrogate it at will. The wave pattern generated by the phased array is the result of the superposition of the waves generated by each individual element. By sequentially firing the individual elements of an array transducer at slightly different times, the ultrasonic wave front can be focused or steered in a specific direction. Thus, sweeping and/or refocusing of the beam is achieved electronically without physically manipulating the transducers. To keep the instrumentation to a minimum, we adopted a virtual steering beam concept. The data collection is conducted in a round-robin pattern. That is to say, at a time, one PWAS serves as transmitter while all the others receive; then all PWASs in the array takes turn to serve as the transmitter. By this means, a total of M^2 signals will be recorded for a M-PWAS array. This set of M^2 elemental signals is then sent to be processed by the EUSR algorithm, implementing the delays and sum as a signal post-processing procedure, such that a virtual sweeping beam is generated. The pulse-echo detection of crack consists of two-step beamforming, the transmission beamforming and reflection beamforming. Hence, the phased array principles are used to image large structural areas from a single location using an array of

M-PWAS in pulse-echo mode. An example of beamforming directivity patterns for an eight-PWAS linear phased array is shown in Fig. 9(*b*). The plot shows the native beamforming (without delays), which for a linear array is at 90 deg, and the directed beamforming at 45 deg after applying appropriate delays.

3.1.2 Frequency Tuning Effects in PWAS EUSR Phased-Arrays. As discussed earlier, Lamb waves can exist in a number of dispersive modes that can simultaneously exist at any given frequency. However, through smoothed tone-burst excitation of carrier frequency f_c and frequency tuning, it is possible to confine the excitation to a particular Lamb wave mode, of wave speed c and wave length λ/f_c. Consider, for example, the structural health monitoring of a thin-wall structure using Lamb waves. For a 1 mm wall thickness and an operation frequency range of 0–1000 kHz, two Lamb wave modes (A0 and S0) exist simultaneously. However, as shown earlier in this paper, there are frequency values where one of the two modes is nearly suppressed. For example, for a 7 mm square PWAS at very low frequency (5–100 kHz), S0 mode vibration is very small and the A0 mode dominates (Fig. 10(*a*)).

Similarly, at frequency 210 kHz, S0 dominates and A0 barely exist. Group velocity frequency plots of S0 and A0 modes are shown in Fig. 10(*b*). We can see that within the 0–1000 kHz range, the S0 mode velocity is almost constant, i.e., the S0 mode is much less dispersive compared to the A0 mode. This observation is consistent with the fact that, usually in Lamb wave nondestructive evaluation (NDE) and SHM applications, A0 mode is used for the detection of surface defects and disbonds/delaminations while S0 mode is used for through the thickness damage detection [8]. Therefore, for crack detection using PWAS phased array, the S0 mode excitation is expected to give much better results. In addition, to obtain a high-quality EUSR scanning image, we also need the response of the S0 Lamb wave mode to be sufficiently strong, thus carrying well the information about damage location and size. Another factor to be concerned during the frequency tuning is the ratio of d/λ. Our previous research has found out that this ratio should be smaller than or equal to 0.5 in order to observe the sampling theorem (otherwise, a disturbing lobe, called the grating lobe, may be present). While within the effective range, a larger d/λ value is desired since it offers better directivity, known as thinner mainlobe width [9]. Scanning with a phased array having good directivity will give a more correct indication of the crack size. Because of the relation $\lambda = c/f$, we see that higher tuning frequency should be used for larger d/λ values. Therefore, the objective of frequency tuning applied to the PWAS phased arrays is to find an excitation frequency high enough and
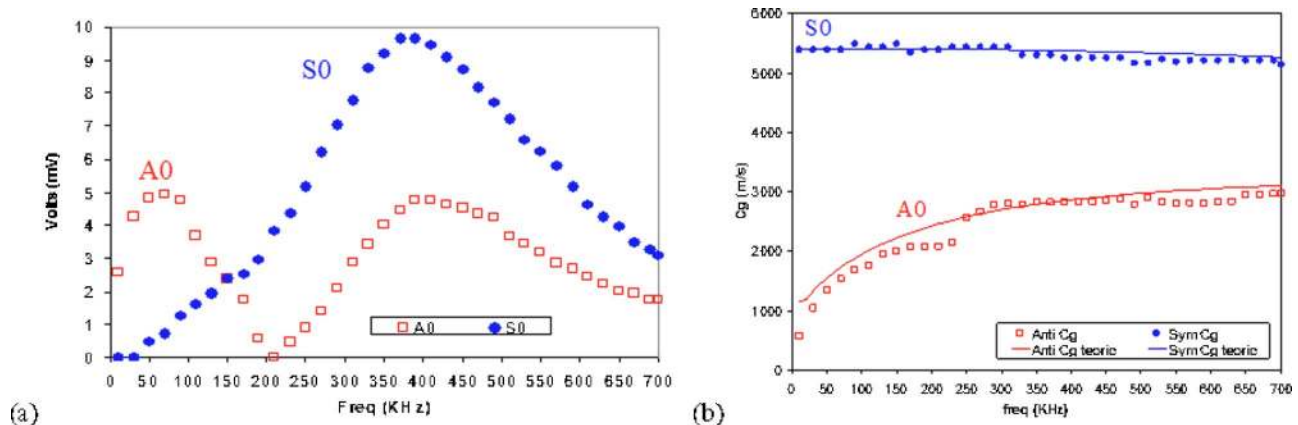

Fig. 10 Frequency tuning for crack detection in a 1 mm thick aluminum plate specimen: (*a*) strain-frequency plot and (*b*) group velocity-frequency plot
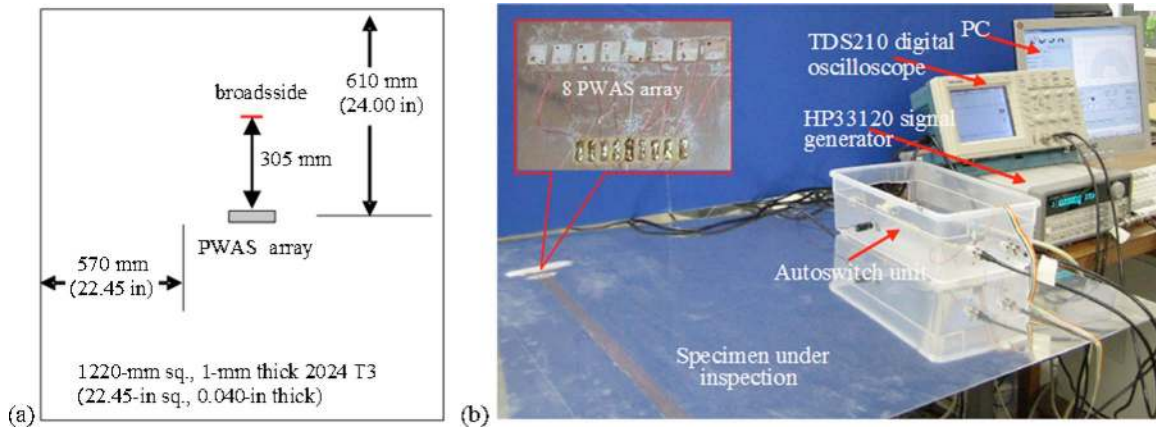
Fig. 11 PWAS guided wave phased array application: (*a*) laboratory specimen layout and (*b*) experiment equipment

at which the response signal will have high S0/A0 ratio (in terms of magnitude), as well as high signal-noise-ratio (SNR) while observing the sampling theorem.

3.1.3 EUSR Phased Arrays With PWAS Frequency Tuning. The specimen used in the experiments was a 1220 mm square 1 mm thick panel of 2024-T3 Al-clad aircraft grade sheet metal stock. The crack is placed on a line midway between the center of the plate and its upper edge. The crack is 19 mm long, 0.127 mm wide. The crack is placed at broadside w.r.t. the phase array at coordinates (0, 0.305 m), i.e., at $r=305$ mm, $\phi_0=90°$ (Fig. 11(*a*)). The PWAS phased array was constructed from eight, 0.2 mm thick, 7 mm square piezoelectric wafers (American Piezo Ceramic Inc., APC-850) placed on a straight line in the center of the plate. The PWAS were spaced at pitch $d=8$ mm. The instrumentation consisted of an HP33120A arbitrary signal generator, a Tektronix TDS210 digital oscilloscope, and a portable PC with DAQ and GPIB interfaces. A LabVIEW™ computer program was developed to digitally control the signal switching, to record the data from the digital oscilloscope, and to generate the group of raw data files. Photographs of the experimental setup are presented in Fig. 11(*b*).

During the Lamb wave-tuning procedure, both pitch-catch and pulse-echo methods were employed to find out the best tuning frequencies. The experimental voltage measurement obtained from pitch catch experiment is shown in Fig. 12(*a*). We see that at frequency 210 kHz, it yields the maximum S0/A0 ratio, whereas at frequency 300 kHz the S0 mode achieves maximum response. Therefore, both 210 kHz and 300 kHz could be used as potential

excitation frequencies. Corresponding theoretical and experimental d/λ values of the S0 mode at various frequencies are listed in Table 2.

To further confirm the frequency tuning, pulse-echo tests were conducted using excitation at 210 kHz and 300 kHz, respectively. Recorded received signals are shown in Figs. 12(*b*) and 12(*c*). By comparing peak-to-peak value of crack echoes, we see that this echo is larger for the 300 kHz frequency (Fig. 12(*a*), point A) than that of the 210 kHz frequency (Fig. 12(*a*), point B). Since the crack echo is the indication of crack presence, the clearer (larger) one is desired. Hence, we choose the 300 kHz over the 210 kHz. After tuning, EUSR experiments are conducted at the tuning frequency 300 kHz and as well at other frequencies (210 kHz and 450 kHz) for further understanding the significance of frequency tuning. EUSR scanning image results are shown in Fig. 13.

At the tuning frequency 300 kHz, we see that the broadside crack was very clearly detected (Fig. 13(*a*)). The image not only indicates the existence of the crack, but also correctly indicates its position on the plate (note: polar coordinate is used in the imaging process). However, using exactly the same experimental setup, the EUSR-generated image at 210 kHz shown in Fig. 13(*b*) cannot clearly identify the existence of the crack, as well as the image obtained at 300 kHz. At this frequency, we have lower d/λ value (see Table 2), which resulted in larger crack shade compared to the higher frequency at 300 kHz. Figure 13(*c*) is the EUSR image at 450 kHz. Though a shade representing the crack image can be seen, it is still much weaker compared to the image obtained at the 300 kHz tuning frequency. By comparison, it can be concluded
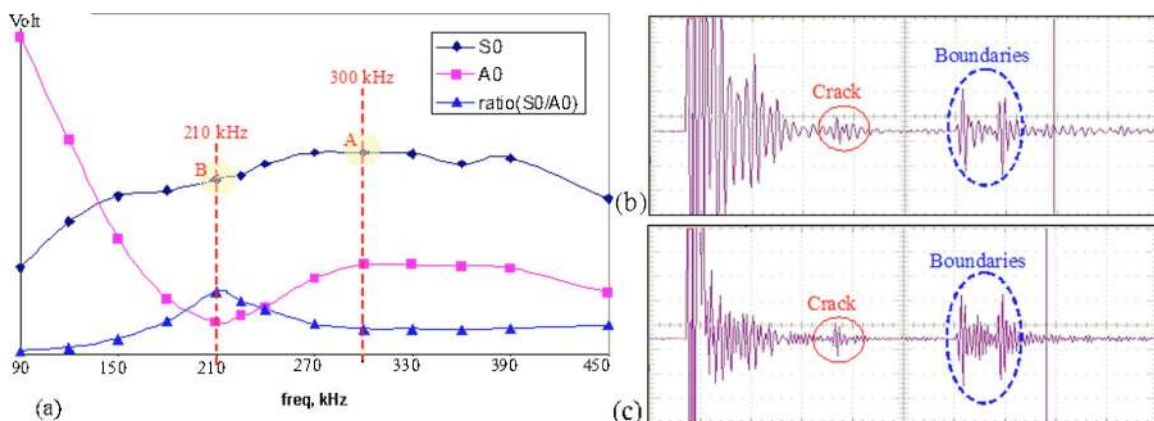

Fig. 12 Frequency tuning for EUSR phased array application: (*a*) pitch-catch voltage measurement, (*b*) pulse echo signal at 210 kHz tuning frequency, and (*c*) pulse echo signal at 300 kHz tuning frequency

Table 2 Theoretical and experimental d/λ values at various frequencies

Frequency, f (kHz)	Theoretical			Experimental		
	c_{S0} (m/s)	λ_{S0} (mm)	d/λ_{S0}	c_{S0} (m/s)	λ_{S0} (mm)	d/λ_{S0}
90	5405	60	0.13	5482	60.9	0.13
120	5403	45	0.18	5435	45.3	0.18
150	5402	36	0.22	5482	36.5	0.22
180	5400	30	0.27	5364	29.8	0.27
210	5397	25.7	0.31	5388	25.7	0.31
240	5394	22.48	0.36	5435	22.6	0.35
270	5391	20	0.4	5435	20.1	0.4
300	5387	18	0.44	5435	18.11	0.44
330	5383	16.3	0.49	5297	16.1	0.5
360	5378	15	0.53	5297	14.7	0.54
390	5373	13.8	0.58	5252	13.5	0.59
450	5361	11.9	0.67	5252	11.7	0.68

that phased array scanning at the 300 kHz tuning frequency offers the best image quality. However, the reader should be aware that for a different specimen and other PWAS types, the tuning frequency would be different, since the specimen material and the thickness, and the PWAS size and dimensions all contribute to the tuning process.

Thus far, the frequency tuning process has been concerned about the S0 mode for crack detection. For A0 mode, the strain plot (Fig. 11) indicates that around 60 kHz, A0 reaches its peaks while S0 is almost suppressed. At this frequency, the corresponding A0 mode wave speed is ~1414 m/s, which results in a d/λ_{A0}

of ~0.34. This is a feasible value for the application of PWAS phased array. Therefore, for other types of damage detection which needs A0 modes, such as corrosion detection, an A0 mode tuning at 60 kHz can be used for the PWAS phased array application. For more details about using S0 mode and A0 mode for different types of damage detection, please refer to [10].

3.2 Time reversal. Time reversal invariance of the acoustic wave equations means that, for every burst of sound diverging from a source—and possibly reflected, refracted, or scattered by any propagation medium—there exists, in theory, a set of waves
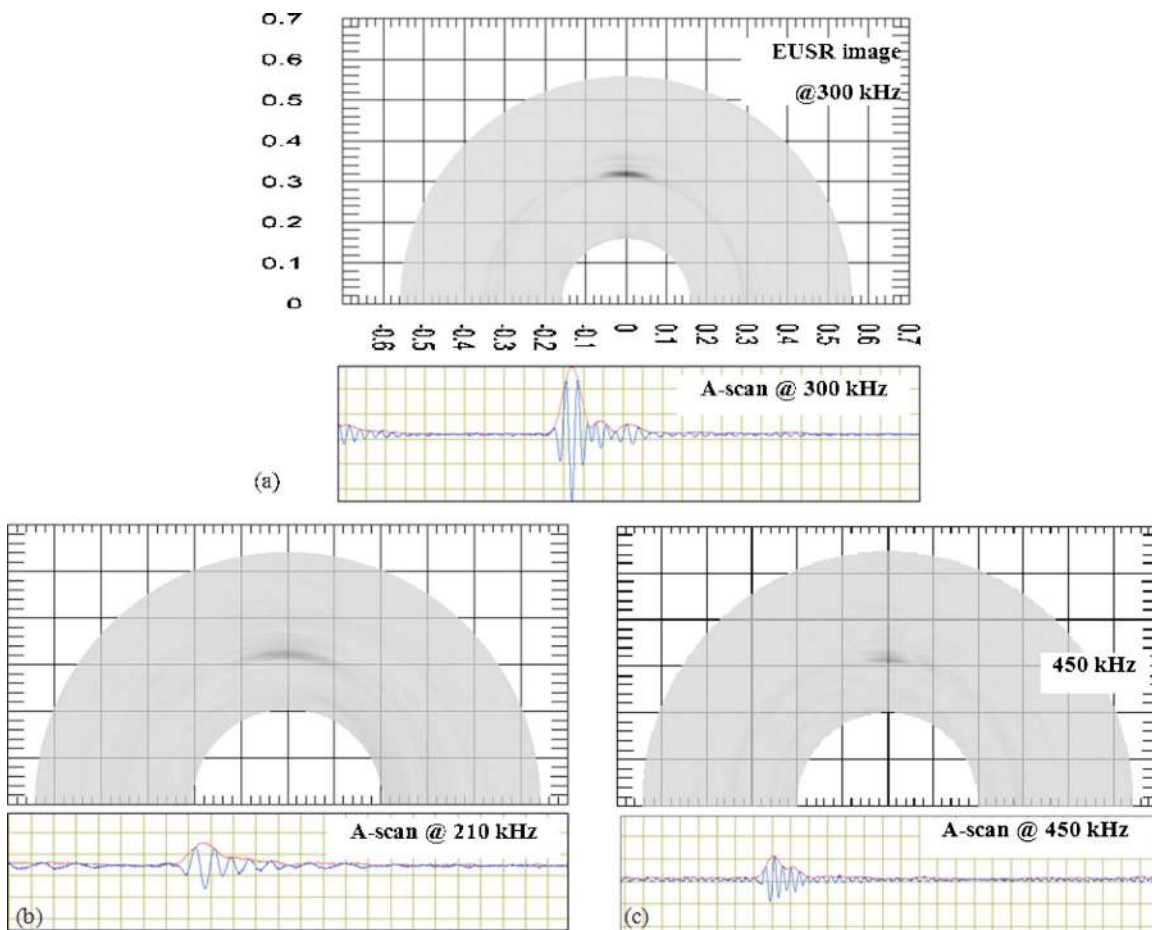

Fig. 13 EUSR inspection using frequency tuning: (*a*) EUSR mapped image at 300 kHz tuning frequency, (*b*) EUSR image at 210 kHz, and (*c*) EUSR image at 450 kHz
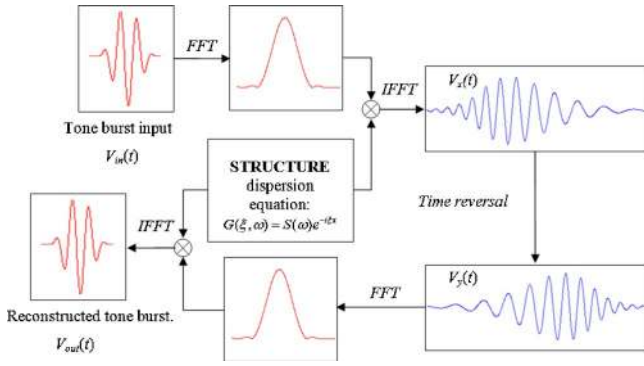
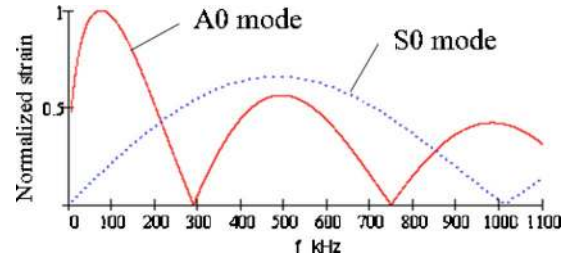Fig. 14   Lamb wave time-reversal procedure block diagram

Fig. 15   Predicted Lamb wave response of a 1 mm aluminum plate under PWAS excitation: normalized strain response for a 7 mm round PWAS (6.4 mm equivalent length)

that precisely retrace all of these complex paths and converges in synchrony, at the original source, as if time were progressing backward. Based on this concept, Ing and Fink [11] presented work on a time-reversal procedure using time-reversal mirror (TRM) to focus energy of a laser-excited Lamb wave on various flaws on a 2D plate. Wang et al. [8] studied time reversal of flexural waves for SHM applications using Mindlin plate theory. They proved that A0 mode dispersive Lamb waves can be recompressed into a tight wave packet through the time-reversal procedure. Kim et al. [12] presented experiments with time-reversal procedure (TRP) as a baseline-free method for damage detection for SHM applications. They observed that when a pair of S0 and A0 Lamb waves is generated, the time-reversal method gives rise to multiple wave packets, i.e., it does not exactly reconstruct the original signal. In this section, we will show that this effect (which hinders the use of time reversal procedure with Lamb wave SHM) can be aleviated through the Lamb wave-tuning method discussed in this paper.

3.2.1 Theory of Lamb Wave Time Reversal. In the time-reversal procedure, an input signal can be reconstructed at an excitation point if an output signal recorded at another point is reversed in time domain and emitted back to the original source point. However, due to dispersive behavior and multimodes characteristic of the Lamb waves, it is difficult to exactly reconstruct the input signal at the excitation point. Figure 14 shows the block diagram of Lamb wave time-reversal procedure.

Computations are first processed in frequency domain to calculate input signal V_{in} and structure transfer function $G(\omega)$, for discrete values of ω. In the second step, an inverse Fourier transform is performed to derive the dispersed forward wave V_x in time domain. Next, this forward wave is time reversed and denoted as signal V_y. Lastly, repeat the first two steps but replace V_{in} with V_y, the input signal is reconstructed as V_{out}. If V_{in} is symmetric, V_{out} is in phase with V_{in}. If V_{in} is asymmetric, the V_{out} should be time reversed to be in phase with V_{in}. The relationship between V_{out} and V_{in} is governed by

$$V_{out}(t) = \text{IFFT}\{Y(\omega) \cdot G(\omega)\} = \text{IFFT}\{V_{in}(-\omega)|G(\omega)|^2\} \quad (11)$$

where IFFT{ } denotes inverse Fourier transform, time-reversal property of Fourier transform was used in the deduction. Note that $|G(\omega)|^2$ is the frequency-dependent transfer function that affects the wave propagation through the medium.

For Lamb waves with only two modes (A0 and S0) excited, the $G(\omega)$ function can be written using Eq. (3) as

$$G(\omega) = S(\omega)e^{-i\xi^S x} + A(\omega)e^{-i\xi^A x} \quad (12)$$

where $S(\omega) = -i(a\tau_0/\mu)\sin(\xi^S a)N_S(\xi^S)/D'_S(\xi^S)$, $A(\omega) = -i(a\tau_0/\mu)\sin(\xi^A a)N_A(\xi^A)/D'_A(\xi^A)$, $\xi = \omega/c$, c represents the phase velocity. Thus,

$$|G(\omega)|^2 = |S(\omega)|^2 + |A(\omega)|^2 + S(\omega)A^*(\omega)e^{-i(\xi^S - \xi^A)x}$$
$$+ S^*(\omega)A(\omega)e^{i(\xi^S - \xi^A)x} \quad (13)$$

where the asterisk denotes complex conjugate, and $|S(\omega)|^2$, $|A(\omega)|^2$ are a series of real numbers. Substiting Eq. (13) into Eq. (11), the first and the second terms on the right-hand side of Eq. (13) will introduce, together, one wave packet at the excitation point, while the third and fourth terms will introduce two extra wave packets in the reconstructed wave V_{out} in the time domain, respectively.

The positions of these extra wave packets can be predicted using Fourier transform property of right/left shift in time. Hence, for the Lamb wave with two modes (S0 mode and A0 mode), the reconstructed wave V_{out} will contain three wave packets. The input signal is not fully reconstructed in this case. This theoretical deduction explains the experimental observations of [12] that were discussed earlier. However, this situation could be alleviated if single-mode Lamb wave could be excited. For the single-mode Lamb wave (e.g., assume S0 mode is dominant after frequency tuning), $G(\omega)$ function can be written as

$$G(\omega) = S(\omega)e^{-i\xi^S x} \quad (14)$$

Thus, V_{out} in Eq. (11) has the same phase spectrum as the time-reversed V_{in} (if V_{in} is symmetric, time-reversed V_{in} is identical to V_{in}), and the magnitude spectrum of V_{out} equals the magnitude spectrum of V_{in} modulated with $|G(\omega)|^2$. For narrowband excitation, $|G(\omega)|^2$ can be assumed to be constant. In this case, V_{out} contains one wave packet representing a perfect reconstruction of the input signal V_{in}. If $|G(\omega)|^2$ varies considerably in the excitation frequency band, the reconstructed signal V_{out} still contains one wave packet but may or may not have a similar shape of the input signal V_{in}.

3.2.2 Time Reversal Simulation of PWAS-Coupled Lamb Waves. We have shown in Sec. 3.2.1 that, in order to fully reconstruct the input Lamb wave signal with the time-reversal procedure, the input signal should be tuned to a frequency point where only one Lamb wave mode is dominant. To achieve this, a narrowband input signal is always preferred.

In our simulation, we considered two 6.4 mm round PWASs, one as transmitter and the other one as receiver, 400 mm apart on a 1 mm aluminum plate. Figure 15 shows the normalized strain plots of Lamb-wave A0 mode and S0 mode of a 1 mm aluminum plate. Note that the strains of two Lamb wave modes are frequency-dependent.

Following the procedure described in Fig. 14, a number of narrowband tone bursts (16-count Hanning windowed) of different carrier frequencies were tested and the input signal was reconstructed using the time-reversal method. Figures 16–18, show the reconstructed waves and residual waves obtained after applying the time reversal method. The input signals were 16-count tone bursts with 500 kHz, 290 kHz, and 30 kHz carrier frequency, respectively. The first frequency corresponds to a case in which both
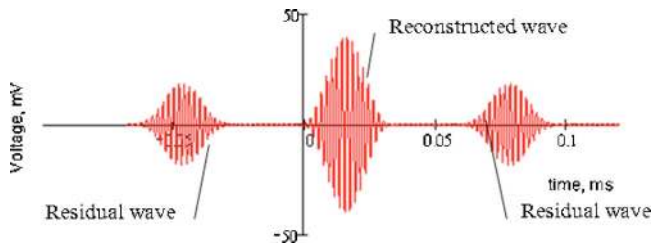
Fig. 16 Untuned time reversal: reconstructed input using 16-count tone burst with 500 kHz carrier frequency. Strong residual signals due to multimode Lamb waves are present.

the A0 and the S0 modes are excited. The second frequency corresponds to a preferential excitation (tuning) of the S0 mode, whereas the third frequency corresponds to the preferential excitation (tuning) of the A0 mode. These three cases are discussed in detail next.

As indicated in Fig. 15, A0 and S0 modes show similar strength around 500 kHz. Therefore, both wave modes are excited by the 500 kHz tone burst. Subsequently, the time-reversed reconstructed wave (Fig. 16) displays two big residual wave packets to the left and right of the reconstructed wave. This is exactly the case observed experimentally by [12]. In contrast, as indicated by Fig. 15, the 290 kHz frequency generates a tuning of the S0 mode., When the S0 mode is dominant, the reconstructed waveform is getting much better with much smaller residual packets. However, as shown in Fig. 17, there are still some small residual wave packets, to the left and right of the main reconstructed wave. The reason for these residual wave packets is that the 16-count tone burst has a finite bandwidth, and hence, a small amplitude residual A0 mode gets excited besides the dominant S0 mode. To eliminate the residual waves, a tone burst with increased count number, i.e., narrower bandwidth, should be used. However, the signal will become long in time duration and lose its resolution in time domain. If we excite with a low frequency, such as 30 kHz, we find from Fig. 15 that the A0 mode is dominant while the S0 mode is very weak. In addition, at these lower frequencies, the bandwidth of the
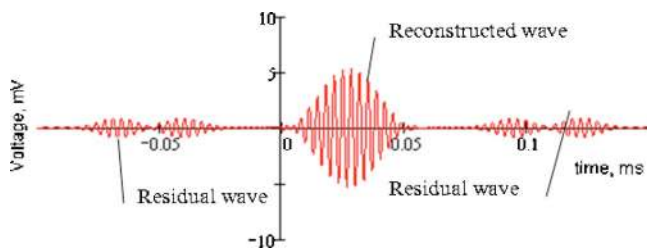

Fig. 17 Time reversal with S0 Lamb wave-mode tuning: reconstructed input using 16-count tone burst with 290 kHz carrier frequency. Weak residual wave packets due to residual A0 mode component are still present due to the side band frequencies present in the tone burst.
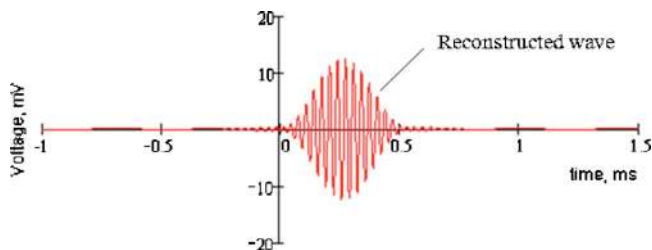

Fig. 18 Time reversal with A0 Lamb mode tuning: reconstructed input using 16-count tone burst with 30 kHz carrier frequency; no residual wave packets are present
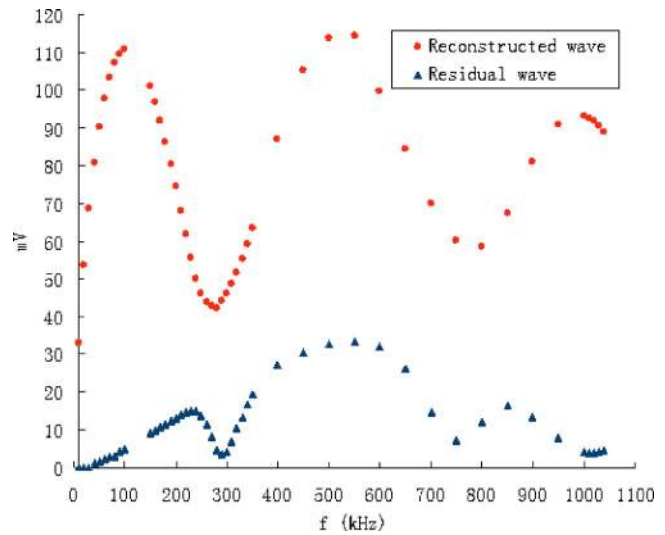

Fig. 19 Reconstructed wave and residual wave in terms of their maximum amplitudes using 16-count tone burst over wide frequency range (10–1100 kHz)

16-count tone burst input signal becomes narrower in actual kilohertz values as compared to the high-frequency bands. Hence, as indicated in Fig. 18, the 30 kHz test signal resulted in a very good reconstruction with the time-reversal method. We see from Fig. 18, that the A0 mode dominates and that the narrowband input signal was perfectly reconstructed by the time-reversal method, with practically no residual wave packets being observed.

Another important fact studied in our simulation was the relative amplitude of the reconstructed wave and the residual wave packets obtained during the time-reversal process at various excitation frequencies. Figure 19 shows the plots of the reconstructed wave packet amplitude and of the residual wave packets amplitudes over a wide frequency range (10–1100 kHz). As it can be seen, for an input signal with a fixed number of counts (here, a 16-count tone burst), the residual wave packet amplitudes vary with respect to input signal tuning frequency. The residual reaches local minimum values and local maximum values at certain tuning frequency points. Hence, the frequency tuning technique can be used to select the optimized input signal frequency that will improve the reconstruction of the Lamb wave input signal with the time-reversal procedure, thus giving a much cleaner indication of damage presence, when damage in the structure is detected through the breakdown of the time-reversal process (for example, for the PWAS size of 7 mm and plate thickness of 1 mm considered in our simulation). Figure 19 indicates that, the 30 kHz, 300 kHz, 750 kHz, and probably the 1010 kHz would be optimal excitation frequencies to be used with the time-reversal damage detection procedure for this particular specimen and PWAS types.

4 Summary and conclusions

This paper has presented a theoretical and experimental study of the Lamb wave frequency tuning with piezoelectric wafer active sensors (PWASs) for use in structural health monitoring (SHM) applications. Since Lamb waves are multimodal, the PWAS transducer can, in principle, excite all Lamb wave modes possible at a given frequency-thickness product. This multimodal aspect can hinder the damage detection process, since many structural health monitor techniques are based on the principle that only one wave mode is present. The first part of the paper has shown how the study of the PWAS interaction with the host structure can lead to methods to preferentially excite/detect only the desired Lamb wave mode or modes. The paper has presented an analytical approach to predicting the PWAS-Lamb wave interaction using the spacewise Fourier transform. This approach allowed

us to predict the amplitudes of each Lamb wave mode as function of frequency, plate thickness and material, and PWAS geometry. Thus, tuning frequencies could be identified at which the response of a particular Lamb wave mode is being either maximized or minimized. Thus, it was shown possible to predict, analytically, the tuning frequencies of a PWAS installed on an isotropic plate and predict the frequencies at which only one particular Lamb wave mode is present. These theoretical predictions were then validated through systematic experiments performed with PWAS of various geometries on plates of different thickness values. The results for square and rectangular shapes installed on 1 mm and 3 mm aluminum alloy plates are being reported in this paper. Comparison between the predicted and measured response curves and tuning frequencies have identified that good agreement can be established between theory and experiments if an effective PWAS size is used. The need for the use of an effective PWAS size resides in the fact that the bonding between the PWAS and structure has finite stiffness, whereas the theory assumed that the bonding was ideal (i.e., infinitely rigid). The effective PWAS size values for various PWAS shapes are given in Table 1.

The second part of the paper has presented a couple applications of the PWAS-Lamb wave tuning. Different SHM techniques rely, to a greater or less extent, on frequency tuning concepts. In this paper, we considered two SHM techniques that benefit greatly from PWAS-Lamb wave tuning: (i) the PWAS phased array method and EUSR imaging, and (ii) the time-reversal method. The PWAS phase array method takes advantage of PWAS-Lamb wave tuning in order to preferentially excite the S0 Lamb wave mode, which is preferred for through crack detection. Our investigations have shown that the desired frequency for optimal crack detection can be determined based on simultaneous satisfaction of two criteria: (i) maximize the S0 Lamb wave response, and (ii) ensure a favorable d/λ ratio for good phased-array performance with avoidance of perturbing side lobes. Using these criteria, both theoretical and experimental tuning have been conducted; it was found that the 300 kHz frequency was optimal for crack detection on a 1 mm thick aluminum plate using an eight 7 mm square PWAS array. To further verify the significance of frequency tuning, the phased array scanning was also conducted at 210 kHz and 450 kHz, and the results showed that only the 300 kHz gave a correct indication of the presence of the crack while the 210 kHz gave a larger image of crack and both 210 kHz and 450 kHz could not give strong and clear crack images.

Time reversal is a method to reconstruct a signal by injecting it back into the structure at the receiving transducer in time-reversed sequence. In SHM applications, the time-reversal process has been advocated [12] as a base-line free method for damage detection base on the premise that the signal reconstruction will breakdown when the structure is damaged. However, due to the multimodal character of the Lamb waves, the time-reversal reconstruction gave multiple signals instead of a single one, as expected [12]. In this paper, we have shown that the success of the time-reversal approach may be strongly dependant on the ability to tune into a single Lamb wave mode. After developing an analytical formulation for the time-reversal process as applied to multimode Lamb waves, the paper has presented a few examples on how tuning can assist the time-reversal reconstruction. First, it was shown that when two Lamb wave modes are present (A0 and S0), the reconstructed signal presents undesired residual wave packets. Then, it was shown that tuning can strongly improve the time-reversal process. Two examples were given: (i) S0 Lamb wave-mode tuning around 290 kHz, and (ii) A0 Lamb wave tuning around 30 kHz. It was shown that mode tuning aleviates the time reversal issues (residual side packets) present at untuned frequencies (e.g., 500 kHz), but this aleviation is perturbed by the fact that even a smoothed tone burst contains sideband frequencies besides the main carrier frequency. These sideband frequencies residually excite the mode that we want to suppress. For this reason, the S0 Lamb wave-mode tuning could not completely eliminate the residual A0 mode packets, while, nevertheless, strongly suppressing them. In contrast, the A0 Lamb wave-mode tuning was found to be much more successful, with virtually no residual S0 modes. (This fact was attributed to the fact that at the A0 tuning frequency the S0 response is generally very weak.)

Overall, this paper has shown that PWAS Lamb wave tuning can be a powerful tool in the implementation of active SHM technology.

References

[1] Crawley, E. F., and de Luis, J., 1987, "Use Of Piezoelectric Actuators as Elements of Intelligent Structures," AIAA J., **25**(10), pp. 1373–1385.
[2] Crawley, E. F., and Anderson, E. H., 1990, "Detailed Models of Piezoceramic Actuation of Beams," J. Intell. Mater. Syst. Struct., **1**, pp. 4–25.
[3] Giurgiutiu, V., 2005, "Tuned Lamb-Wave Excitation and Detection With Piezoelectric Wafer Active Sensors for Structural Health Monitoring," J. Intell. Mater. Syst. Struct., **16**(4), pp. 291–305.
[4] Raghavan, A., and Cesnik, C. E. S., 2004, "Modeling of Piezoelectric-Based Lamb-Wave Generation and Sensing for Structural Health Monitoring," Proc. SPIE, **5391**, pp. 419–430.
[5] Raghavan, A., and Cesnik, C. E. S., 2005, "Piezoelectric-Actuator Excited-Wave Field Solution for Guided-Wave Structural Health Monitoring," Proc. SPIE, **5765**, pp. 313–323.
[6] Auld, B. A., 1990, *Acoustic Fields and Waves in Solids*, Wiley, New York, Vol. 1 and 2.
[7] Giurgiutiu, V., and Bao, J., 2002, "Embedded-Ultrasonics Structural Radar for the Nondestructive Evaluation of Thin-Wall Structures," *Proc. of 2002 ASME International Mechanical Engineering Congress*, Nov. 17–22, New Orleans, ASME, New York, ASME Paper No. IMECE2002–39017.
[8] Wang, C. H., Rose, J. T., and Chang, F. K., 2004, "A Synthetic Time-Reversal Imaging Method for Structural Health Monitoring," Smart Mater. Struct., **13**(2), pp. 415–423.
[9] Yu, L., and Giurgiutiu, V., 2006 "Damage Detection Using Guided Waves and Piezoelectric Wafer Active Sensor Arrays," Proc. of IMAC XXIV, 30 Jan.–2 Feb., St. Louis, MO, Paper No. 170 (CD-ROM).
[10] Giurgiutiu, V., Bao, J., and Zhao, W., 2003 "Piezoelectric-Wafer Active-Sensor Embedded Ultrasonics in Beams and Plates," Exp. Mech., **43**(4), pp. 428–449.
[11] Ing, R. K., and Fink, M., 1998, "Time Reversal Lamb Waves," IEEE Trans. Ultrason. Freq. Control, **45**(4), pp. 659–663.
[12] Kim, S., Sohn, H., Greve, D., and Oppenheim, I., 2005, "Application of a Time Reversal Process for Baseline-Free Monitoring of a Bridge Steel Girder," International Workshop on Structural Health Monitoring, Stanford, CA, Sept. 15–17.